JCSE Journal of Computing Science and Engineering

Regular Paper

Journal of Computing Science and Engineering,
Vol. 8, No. 2, June 2014, pp. 119-128

Automatic Segmentation of Retinal Blood Vessels Based on Improved Multiscale Line Detection

Yanli Hou*

School of Computer and Information Technology, Shangqiu Normal University, Shangqiu, China **xjgao75@163.com**

Abstract

The appearance of retinal blood vessels is an important diagnostic indicator of serious disease, such as hypertension, diabetes, cardiovascular disease, and stroke. Automatic segmentation of the retinal vasculature is a primary step towards automatic assessment of the retinal blood vessel features. This paper presents an automated method for the enhancement and segmentation of blood vessels in fundus images. To decrease the influence of the optic disk, and emphasize the vessels for each retinal image, a multidirectional morphological top-hat transform with rotating structuring elements is first applied to the background homogenized retinal image. Then, an improved multiscale line detector is presented to produce a vessel response image, and yield the retinal blood vessel tree for each retinal image. Since different line detectors at varying scales have different line responses in the multiscale detector, the line detectors with longer length produce more vessel responses than the ones with shorter length; the improved multiscale detector combines all the responses at different scales by setting different weights for each scale. The methodology is evaluated on two publicly available databases, DRIVE and STARE. Experimental results demonstrate an excellent performance that approximates the average accuracy of a human observer. Moreover, the method is simple, fast, and robust to noise, so it is suitable for being integrated into a computer-assisted diagnostic system for ophthalmic disorders.

Category: Smart and intelligent computing

Keywords: Image segmentation; Retinal image; Morphological processing; Multiscale line detection

I. INTRODUCTION

Inspection of the retinal blood vessels can reveal early stages of hypertension, diabetes, arteriosclerosis, cardiovascular disease, and stroke [1]. It allows the patients to take action while the disease is still in its early stages. One nontrivial task in the diagnosis of retinopathy is the segmentation of retinal blood vessels [2]. However, since the vascular network is complex and the number of images is large, the manual segmentation of retinal blood vessels can become a time-consuming process that entails training and skill. An automated segmentation method provides consistency and accuracy, and reduces the time taken by a physician or a skilled technician for hand mapping. Therefore, an automated reliable method for vessel segmentation would provide valuable computer-assisted diagnosis for ophthalmic disorders.

Feature characterization and extraction in retinal images is, in general, a complex task [3]. Accurate blood vessel segmentation is a difficult task for several reasons. The challenges include low contrast; the presence of noise influence, mainly due to its complex acquisition; and anatomic variability, depending on the particular patient. The variability of vessel width, brightness, and tree-like shape

Open Access http://dx.doi.org/10.5626/JCSE.2014.8.2.119 http://jcse.kiise.org

Received 23 November 2013; **Revised** 28 May 2014; **Accepted** 2 June 2014

*Corresponding Author

 pISSN: 1976-4677 eISSN: 2093-8020

make the task more difficult. For example, two close vessels are often considered as one wide vessel. In contrast, a vessel with central light reflex may be misunderstood as two vessels [4]. Further challenges faced in automated vessel segmentation include the presence of low-contrast small vessels, and the appearance of a variety of structures in the image, including the optic disk, retinal boundary, lesions, and other pathologies [5].

Many methodologies for retinal vessel segmentation have been reported. Reviews and surveys of these methods can be found in [6, 7]. All these approaches for detecting retinal blood vessels can be classified into techniques based on match filtering, morphological processing, vessel tracking, pattern recognition, multiscale analysis, and model-based algorithms [8]. Matched filters for retinal vessel segmentation exploit the piecewise linear approximation, and the Gaussian-like intensity profile of retinal blood vessels [9]. Vessel segments are searched in all possible directions, using a two-dimensional matched filter. Mathematical morphology exploits the fact that the vessels are linear, connected, and their curvature varies smoothly along the crest line to highlight the vessels in the monochromatic retinal image [10]. Vessel tracking methods track the vessels, starting from a set of reliable seed points, using local information of the vessel network [11]. The multiscale approaches for vessel extraction are based on scale-space analysis, separating out information related to the blood vessels having varying width [12]. Model-based methods utilize the vessel profile models and active contour models, and have been introduced for accurate estimation of vessel width. An example is the tramline filter proposed by Hunter et al. [13], where two parallel edges at variable distance from each other are expected to detect a vessel locally. The tramline filter consists of three parallel lines, where the inner line is aligned within a blood vessel, and the outer two lines are just on either side of the vessel; the filter gives a strong response. Thus, the tramline is more suited to the detection of vessel centerlines than to segmentation of the vessels. Similar to the tramline filter, a line detector is proposed by Ricci and Perfetti [14]. The line detector evaluates the average pixel intensity along basic lines passing through the target pixel at different orientations, and selects the line with the highest average pixel intensity, so as to detect vessels from the retinal images. The basic line detector with long lines is effective in dealing with the vessels with central reflex. But its length is fixed; when two vessels are very close, it will merge them.

This drawback can be avoided by using the generalized multi-scale line detector proposed by Nguyen et al. [4]. They use variable lengths of aligned lines, instead of a fixed one, to achieve a multi-scale line detector. The longer length line detectors are effective in dealing with central reflex, but tend to merge close vessels, and produce false responses at vessel crossovers. The shorter length line detectors can improve these situations, but introduce background noise to results. In order to preserve the strength and overcome the drawback of each individual line detector, Nguyen et al. [4] assign the same weight for each line detector with different length, and linearly combine all line responses at different scales to get the vessel responses. Clearly, the contributions of line responses at different scales to final segmentation are not equal. The longer length line detectors can get more vessel responses than the shorter ones. Simple assignment of the same weight for each scale to combine all the line responses will introduce much background noise to final segmentation. Nguyen et al.'s multiscale line detector gives false responses around the optic disk and pathological regions, such as dark and bright lesions. An example is illustrated in Fig. 1.

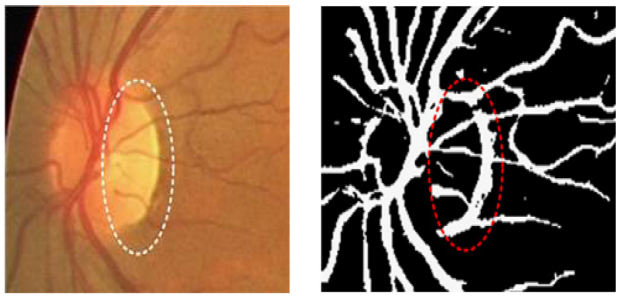

Fig. 1. False vessel detection around the optic disk in Nguyen et al. [4]'s multiscale line detector: (a) original image and (b) segmented image. Adapted from Nguyen et al. [4] with permission.

To overcome the drawbacks mentioned above, this paper proposes an effective retinal blood vessel segmentation methodology. Exploiting the properties of piecewise linearity and connectedness of the retinal vessel, we have introduced multi-director morphological filters with rotating structuring elements to enhance the vessels in the ocular fundus image. Later, an improved multiscale line detector is proposed to produce the vessels response. Our method is quantitatively and qualitatively evaluated using two publicly available data sets, DRIVE [15] and STARE [16]. In comparison with Nguyen's multiscale line detection method and the basic line detection, the algorithm attains excellent performance. Receiver operating characteristic (ROC) analysis is also used on the three detectors. From the area under the ROC curve and the accuracy, we can see that our approach works extremely well, while approximating the average accuracy of a human observer without a significant degradation in sensitivity and specificity.

The rest of the paper is organized as follows. Section II is the preliminary knowledge about line detection; two line detectors for retinal vessel segmentation are briefly mentioned. In Section III, we illustrate our proposed methodology in detail. Experimental results on the images of the DRIVE and STARE databases are presented in Sec-

tion IV. Finally, Section V presents the conclusion of this paper.

II. MULTISCALE LINE DETECTION

Multiscale line detection proposed by [4] is built upon the basic line detector, which is first used as a means for vessel-background classification by [14]. In this section, we first review the basic line detector, and then introduce multiscale line detection, which linearly combines all line responses at varying scales to produce the final segmentation for a retinal image.

A. Basic Line Detector

The retinal vasculature appears as piecewise linear features with variation in width and their tributaries visible within the retinal image. The basic line detector employs the morphological attributes of retinal blood vessels to produce vessel responses. It works on the inverted green channel of original RGB images, where the vessels appear brighter than the background. First, a square sub window of size $W \times W$ pixels is centered at each pixel position in the retinal image. Then, the average of pixel intensities, termed I_{avg}^{W}, is computed. That is, twelve lines of length W pixels oriented at 12 different directions (angular resolution of 15°) passing through the centered pixels are identified, and the average of gray levels of pixels along each line is computed. The line with the highest average is called the 'winning line', and its value is defined as $I_{\max}^{W}$. The line response at the centered pixel is then computed as [14]:

$$R_W = I_{\max}^{W} - I_{avg}^{W} \tag{1}$$

where, the window size W should be chosen to ensure that the window of the pixel at the center of the vessels consists of an approximately equal number of vessels and background pixels.

The basic line detector principle is that if the target pixel belongs to the vessel, then the line response will be large due to alignment of the candidate line along the direction of the vessel. In contrast, the line response is low for a background pixel, because the difference between the pixel intensity of the candidate line and square sub-window is small. In this basic line detector, the window size is chosen in such a way that if the square sub-window is placed on the image, and the center of this window corresponds to the center of the vessel, then this window contains approximately the same number of vessel and background pixels. Therefore, it is often set as twice the typical vessel width in retinal images. For example, it has been shown that $W = 15$ is a good choice for the DRIVE database, where the typical vessel width is 7–8 pixels [15].

The basic line detector has been shown to be effective when dealing with vessels with central light reflex. However, there are three drawbacks of using it in vessel detection: 1) it tends to merge close vessels; 2) it produces an extension at crossover points; and 3) it produces false vessel responses at background pixels near strong vessels (vessels with high intensity values in images where vessels appear brighter than the background).

B. Multiscale Line Detection

To overcome the three drawbacks of the basic line detector mentioned above, Nguyen et al. [4] proposed a generalized multiscale line detector, which uses a variable length of aligned lines in spatial scale. The generalized multiscale line detector is defined as [4]:

$$R_W^L = I_{\max}^{L} - I_{avg}^{W} \tag{2}$$

where, $1 \le L \le W$, $I_{\max}^{L}$ and I_{avg}^{W} are defined as in Eq. (1). By changing the values of L, the multiscale line detector can be obtained. Fig. 2 depicts a line detector with $W = 15$ and $L = 9$, where 12 lines of 9 pixel length are placed on top of a window of 15 × 15 pixels. The main idea behind this is that the shorter length line detector will avoid the inclusion of surrounding vessel pixels, and hence give correct false responses to closely located vessels, and at vessel crossovers.

In multiscale line detectors, the line responses at different scales are different. The longer length line detector can detect large diameter blood vessels, and be able to deal with central reflex, because the candidate line includes only a small number of central reflex pixels, which would not have been much affected, so the central reflex pixels have a high vessel response. The shorter length line detector detects close vessels more effectively.

In order to maintain the strength and eliminate the

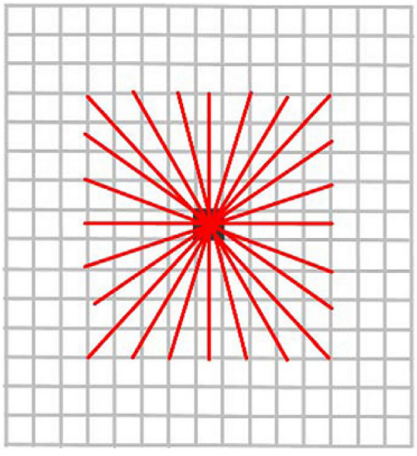

Fig. 2. A generalized line detector with $W = 15$ and $L = 9$. Adapted from Nguyen et al. [4] with permission.

drawback of each individual line detector, the final vessel responses are obtained by the linear combination of line responses computed by using line detectors at different scales. The response at each image pixel is defined as:

$$R_{combined} = \frac{1}{n_L + 1}\left(\sum_L R_W^L + I_{igc}\right) \quad (3)$$

where n_L is the number of scales used, R_W^L is the response of the line detector with line length L and square sub-window W, and I_{igc} is the inverted green channel image at the corresponding pixel. The original green channel is included in the combination, since it provides additional information to discriminate the proximity between the blood vessels and other structures, such as pathologies and the optic disk.

III. PROPOSED METHODOLOGY

Our proposed methodology for retinal blood vessel segmentation comprises of 4 consecutive stages: 1) image preprocessing for background homogenization and the removal of noise; 2) vessel enhancement using multi-director morphological filters with linear structuring elements; 3) improved multiscale line detection for getting vessel response; and 4) post-processing for removing artifacts. Note that when the RGB components of the colored retinal images are visualized separately, the green channel shows the best vessel/background contrast; whereas the red and blue channels show low contrast and are very noisy [15]. Therefore, the green channel is used for processing by our method.

A. Preprocessing

Independently from the component derived from the original color retinal images, our proposed segmentation method works on the inverted green channel (I_g) of a retinal image, so that the vessels appear brighter than the background. An example of an inverted green channel image is shown in Fig. 3(a).

Our multiscale line detection responds strongly to high contrast edges. It may lead to false detection around the borders of the camera's aperture. In order to reduce this effect, an iterative algorithm developed by [17] is used to remove the strong contrast between the retinal fundus and the region outside the camera's field of view (FOV). The result of the iterative process is illustrated in Fig. 3(b).

Retinal images often contain background intensity variation, since the illumination is reduced, while the distance to the optic disk is increased. Consequently, background pixels may have different intensity for the same image. We can see this in Fig. 3(a), where the intensity values of some background pixels are comparable to that of brighter vessel pixels. This makes it difficult to segment retinal vessels. With the purpose of removing these background lighting variations, a background homogenization method proposed by [18] is described, as follows.

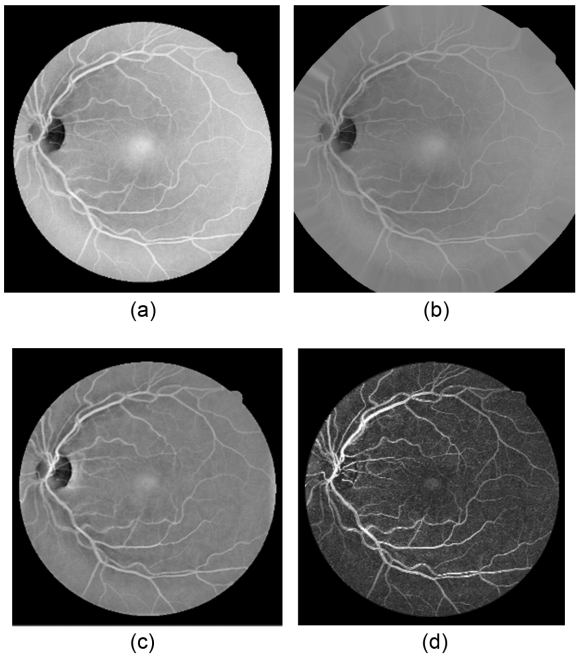

Fig. 3. Illustration of the preprocessing process: (a) inverted green channel image, (b) preprocessed image with extended border, (c) homogenized image, and (d) enhanced vessels image from sum of top-hat transformation.

First, a 3 × 3 mean filter is applied to smooth occasional salt-and-pepper noise. Then, the resultant image is convolved with a Gaussian kernel of dimensions $m \times m = 9 \times 9$, mean $\mu = 0$, and variance $\sigma^2 = 1.8^2$, which can further smoothen noise effectively. Second, a background image I_B is produced by applying a 59 × 59 mean filter. Then, the difference between I_g and I_B is calculated for every pixel, and the result of background homogenization is shown in Fig. 3(c), where the influence of the background of retinal images is decreased.

B. Vessel Enhancement

The purposes of vessel enhancement are to eliminate the influence of the optic disk and to increase vascular contrast from the background of the retinal image. In our segmentation method, morphological operators with directional structuring elements are applied to enhance the vessel contrast in the homogenized image I_D.

The retinal vessels appear as linear bright shapes in the monochromatic image I_D, and can easily be identified using mathematical morphology. The basic morphological operations of erosion, dilation, and opening and closing with a structuring element are defined in [19]. Morphological opening using a linear structuring element oriented at a particular angle will eradicate a vessel or

part of it, when the structuring element cannot be contained within the vessel. This happens when the vessel and the structuring element have orthogonal directions, and the structuring element is longer than the vessel width. Conversely, when the orientation of the structuring element is parallel to the vessel, the vessel will stay nearly unchanged. The morphological top-hat transformation is shown as:

$$I_{th}^{\theta} = I - (IoS^{\theta}) \tag{4}$$

where I_{th}^{θ} is the top-hat transformed image, I is the image to be processed, S represents structuring elements for morphological opening, and θ is the angular rotation of the structuring element. If the opening along a class of linear structuring elements is considered, a sum of top-hats along each direction will brighten the vessels, regardless of their direction, provided that the length of the structuring elements is large enough to extract the vessel with the largest diameter. Therefore, a set of line structuring elements, where each one is a matrix representing a line of 21 pixels in length, and each rotated at 22.5°, is used for the morphological top-hat transformation. Its size is approximately the range of the diameter of the biggest vessels for retinal images. The sum of the top-hats is depicted as:

$$I_{th} = \sum_{\theta \in A} I_{th}^{\theta} \tag{5}$$

where I_{th} is the sum of top-hat transformation performed with the structuring element oriented at θ degrees. The set A is denoted as $\{x | 0 \le x \le 180,\ x \bmod (22.5) = 0\}$. In the image, every isolated round and bright zone whose diameter is less than the length of the linear structuring element pixels has been removed. The sum of top-hats on the image will enhance all vessels, whatever their direction is, including small or tortuous vessels. The normalized image I_{ve} after top-hat transformation is shown in Fig. 3(d). Here, we can see that the influence of the optic disk is removed, because the optic disk is not a linear structure, so that it is not enhanced.

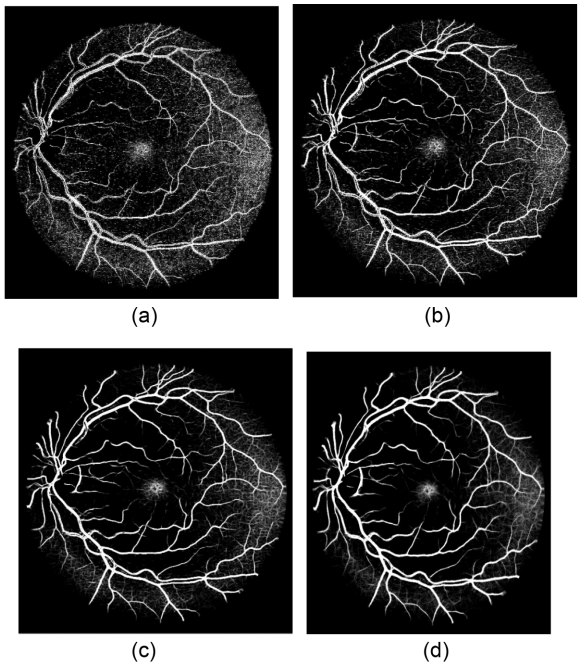

Fig. 4. Vessel responses using line detectors at different scales. (a) $L = 3$, (b) $L = 5$, (c) $L = 9$, and (d) $L = 15$.

C. Improved Multiscale Line Detection

In this section, we propose an improved multiscale line detection, to obtain the final vessel measure from the enhanced retinal vessels. In Nguyen et al.'s multiscale line detectors, different line detectors have different line responses. The line detector with longer lines can successfully recognize central reflex pixels as vessel pixels, because the candidate line includes only a small number of central reflex pixels; hence the average intensity of pixels in the candidate line is not much affected, and the central reflex pixels have a high vessel-ness measure. The shorter length line detectors detect close vessels more effectively, but introduce background noise into the image.

Fig. 4 illustrates the vessel responses using line detectors at different scales. Here we can see that the longer length line detectors produce more vessel responses. Although the shorter length line detectors can provide more vessel details, they are sensitive to noise. The variances of line responses at different scales to image noise are depicted in Fig. 5, which demonstrates that the smaller scale filters produce higher noise responses. In order to maintain the strength and eliminate the drawback of each individual line detector, line responses at different scales are linearly combined to produce the segmentation for each retinal image. We assign different weights for each scale, and the response at each image pixel is defined as:

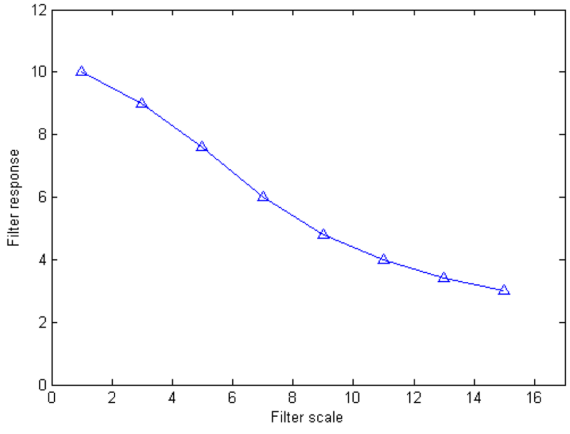

Fig. 5. Variances of responses to noise along scale space.

$$R_{combined} = \frac{1}{n_L + 1}\left(\frac{1}{n_L}\sum_{L} L * R_W^L + I_{ve}\right) \quad (6)$$

where n_L is the number of scales used, R_W^L is the response of the line detector at scale L, and I_{ve} is the enhanced image. Since I_{ve} includes more blood vessels information, we use it to replace the inverted green channel image [4].

D. Post-processing

The combined line response image is a soft classification, where each value represents the probability of each pixel of belonging to the vessel class. A single threshold is enough to segment the soft classification, and produce a binary segmentation (Fig. 6(a)). There are many small isolated regions misclassified by threshold segmentation as blood vessel pixels. To improve segmentation performance, the removal of falsely detected isolated vessel pixels is processed. In order to remove these artifacts, the pixel area in each connected region is measured. In artifact removal, each region connected to an area below 25 is reclassified as non-vessels. An example of the final vessel segmented image after this further processing stage is shown in Fig. 6(b).

IV. EXPERIMENTAL EVALUATION

A. Materials

We evaluated our retinal vessel segmentation methods on two publicly available data sets. Both the DRIVE database and the STARE database have been widely used by researchers to test their vessel segmentation methodologies, since they provide manual segmentations for performance evaluation.

The DRIVE database [15] contains 40 color fundus images, which have been divided into a test set and a training set, both containing 20 images. Each of the twenty training images has been carefully labeled by an expert, by hand, to produce ground truth vessel segmentation. For the test cases, two manual segmentations are available; one is used as a gold standard, and the other can be used to compare computer generated segmentations with those of an independent human observer. The images were acquired using a Canon CR5 non-mydriatic 3CCD camera with a 45° FOV. Each image was captured using 8 bits per color plane at 768 by 584 pixels. The FOV of each image is circular with a diameter of approximately 540 pixels. For this database, the images have been cropped around the FOV. For each image, a mask image is provided that delineates the FOV.

The STARE database [16] contains 20 colored retinal images, with 700 × 605 pixels and 8 bits per RGB channel, captured by a TopCon TRV-50 camera at a 35° FOV. Two manual segmentations by Hoover and Kouznetsova [16] are available. The first observer marked 10.4% of the pixels as vessel, the second one 14.9%. The performance is computed with the segmentations of the first observer as a ground truth. The comparison of the second human observer with the ground truth images gives a detection performance measure, which is regarded as a target performance level.

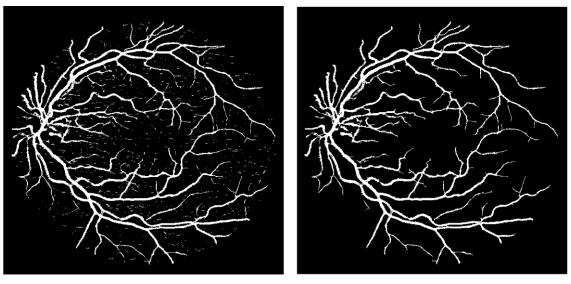

(a) (b)

Fig. 6. Results of segmentation: (a) threshold segmentation and (b) post-processing image.

B. Performance Measures

In order to quantify the algorithmic performance of the proposed method on a fundus image, the resulting segmentation is compared to its corresponding ground truth image. Any pixel that is identified as a vessel in both the ground truth and the segmented image is marked as a true positive (TP). Any pixel that is marked as a vessel in the segmented image, but not in the ground truth image, is counted as a false positive (FP), as illustrated in Table 1.

In this paper, our algorithm is evaluated in terms of sensitivity, specificity, and accuracy. Sensitivity is the ability of an algorithm to detect the vessel pixels. Specificity reflects the ability to detect non-vessel pixels. The accuracy is measured by the ratio of the total number of correctly classified pixels (sum of TPs and TNs) by the number of pixels in the image FOV. Taking Table 1 into account, these metrics are defined as:

$$Sensitivity = \frac{TP}{TP + FN} \quad (7)$$

$$Specificity = \frac{TN}{TN + FP} \quad (8)$$

$$Accuracy = \frac{TP + TN}{TP + FP + TN + FN} \quad (9)$$

Table 1. Vessel classification

	Vessel present	Vessel absent
Vessel detected	True positive	False positive
Vessel not detected	False negative	True negative

Since more than 80% of pixels in a retinal image FOV are background, the accuracy is always high, and there is only a small discrimination in the accuracy values of different methods. In this paper, a Local Accuracy is introduced as an additional measure, according to [4]. Here, only vessels and background pixels around the true vessels are evaluated for accuracy measurement. To achieve this, the ground truth segmentation image is dilated using a morphological dilation operator with a structure element of size S, and this dilated image is used as the mask for accuracy measurement. The Local Accuracy of different methods is reported with $S = 3$, since at this value, an equal number of vessels and background pixels is considered for accuracy computation.

In addition, algorithm performance is also measured with ROC curves. An ROC curve plots the fraction of vessel pixels correctly classified as vessels, namely the true positive rate (TPR), versus the fraction of non-vessel pixels wrongly classified as vessels, namely the false positive rate (FPR). TPR represents the fraction of pixels correctly detected as vessel pixels. FPR is the fraction of pixels erroneously detected as vessel pixels. The area under the ROC curve (AUC) measures the ability of the classifier to correctly distinguish between vessel and non-vessel pixels. The closer the curve approaches the top-left corner, the better is the performance of the system. For both databases, TPR and FPR are computed, considering only pixels inside the FOV.

C. Vessel Segmentation Results

In this section we first report qualitative results that are aimed at giving a visual feeling of the quality of the retinal blood vessel tree generated by our method. We then report comparative, quantitative results, using several performance parameters and the standard ROC method. We compare our improved multiscale line detection with the other two line detectors: basic line detector of Ricci and Perfetti [14] and multiscale line detector of Nguyen et al. [4].

The parameter setting of our method on these experimental databases is simple. Since the vessel width in these images is around 7–8 pixels, W is set to 15 pixels, and the scale range of the line detectors is set to 8 from 1 to 15 with a step of 2. The vessel responses obtained by improved multiscale line detection are a soft classification, where each value represents the probability of each pixel belonging to the vessel class. A single threshold can segment the soft classification, and produce binary segmentation for each retinal image. In order to choose the threshold value, 20 images in the DRIVE training set are used to tune the threshold parameter. The threshold value that produces the highest average accuracy on the training set is at $t = 0.56$. Hence, the same threshold value of $t = 0.56$ is used to segment all images in the DRIVE and STARE databases.

Figs. 7(a) and (b) show the segmentation results of one image in the DRIVE data set obtained by Nguyen et al.'s method and our method, respectively. Here we can see that both methods have the ability to recognize the vessels with the center of central reflex, and can segment these close vessels. Compared to Fig. 7(a), our results (Fig. 7(b)) show two improvements: 1) most of the FP results around the optic disk are detected, as shown by the green circle area; and 2) the vessel blood tree gained from our methods includes more small vessels. An explanation for these improvements is the multidirectional morphological top-hat transform incorporated in our method, which enhanced the vessel, and removed the influence of the optic disk.

Vessel segmentation results of one image each from the DRIVE and the STARE databases are illustrated in Fig. 8. The figures illustrate the green channel of the fundus image, the manually segmented images from the first human observer, the segmented results of Nguyen et al.'s method, and the vessel tree yield from our method. Compared to the results of Nguyen et al.'s method, our vessel tree not only removes the optic disk, but also includes more small vessels. The improved multiscale line detector proposed in our method sets different weights to each line response, according to the lengths of the line detectors. The weight of the shorter line detectors is lower, so the vessel responses include less background noise, which could yield segmentation results with more vessel details, after simple post-processing.

Fig. 9 illustrates another two segmentation results of one pathological retinal image each from the DRIVE and the STARE databases. Compared to Nguyen et al.'s method, our proposed method can obtain more details of retinal vessels, even in the area of the optic disk and pathological lesions. Since the multidirectional filters can remove every isolated round and bright zone whose diameters are less than the length of the linear structuring element pixels, the influence of the optic disk and pathological lesions for vessel detection is decreased.

The ROC curves of the three line detection methods for the two databases are depicted in Figs. 10 and 11, where the AUC values of our proposed method are

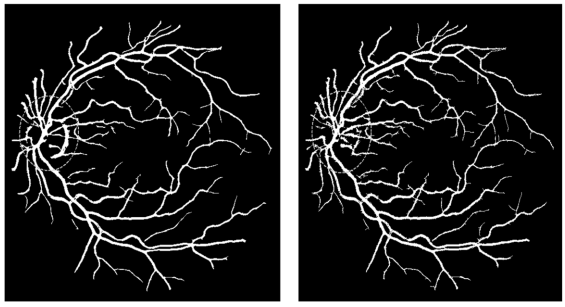

Fig. 7. Results of segmentation: (a) Nguyen et al.'s method and (b) our method.

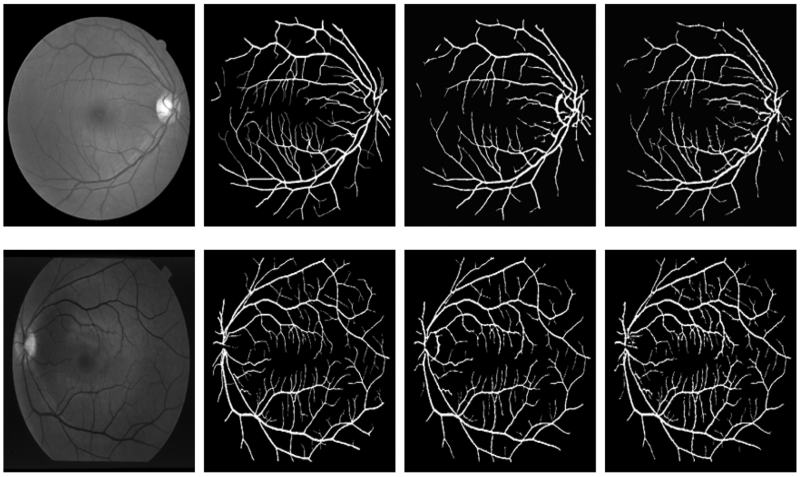

Fig. 8. Comparative results of two different methods: (a) original image, (b) ground truth image, (c) Nguyen et al.'s method, and (d) our method.

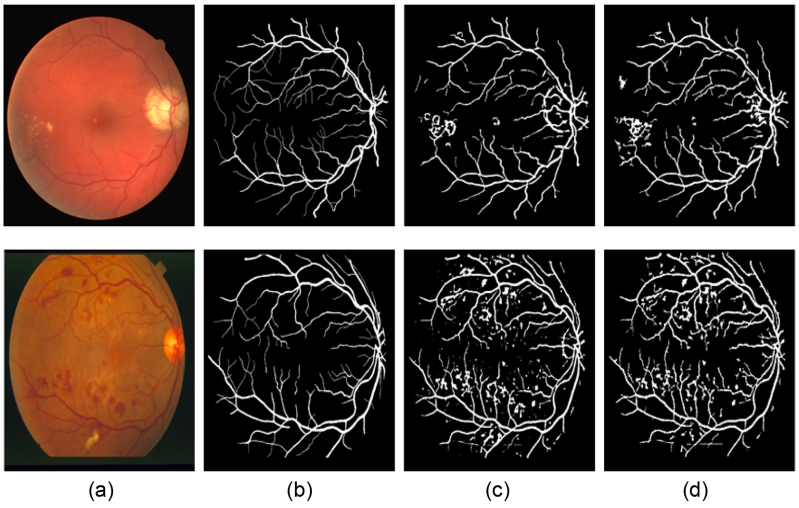

Fig. 9. Segmentation results of pathological retinal image: (a) original image, (b) ground truth image, (c) Nguyen et al.'s method, and (d) our method.

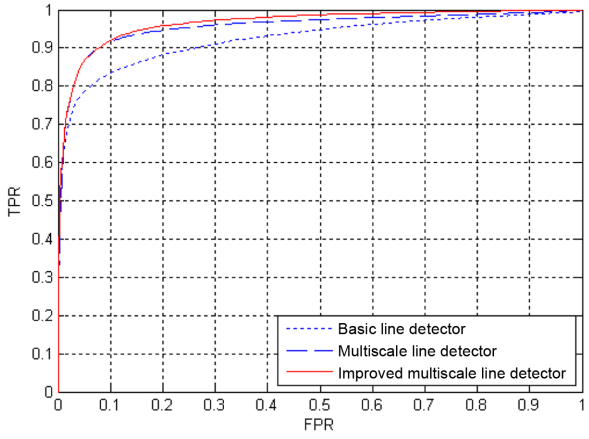

Fig. 10. Receiver operating characteristic curves for the DRIVE database. TPR: true positive rate, FPR: false positive rate.

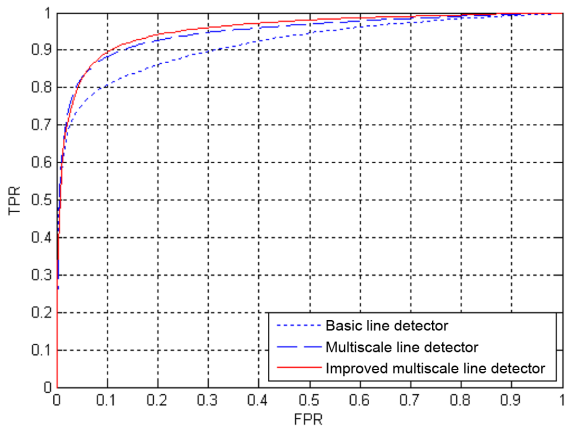

Fig. 11. Receiver operating characteristic curves for the STARE database. TPR: true positive rate, FPR: false positive rate.

0.9618 and 0.9576 for the DRIVE and STARE databases, respectively. The ROC curves of the basic line detector are obtained from the line detector with line length $L = 15$, which achieves the maximum average accuracy, compared to other length line detectors [14].

Tables 2 and 3 present the average performance of the three line detectors on both DRIVE and STARE data sets. Since the segmentation results of the basic line detector are not available for comparison, we implemented the unsupervised method, denoted as individual line detection with line length $L = 15$. The results show that the accuracy of improved multiscale line detection is higher than that of individual line detection, since they combined all line responses, and eliminated the drawback of each individual line detector. However, Nguyen et al.'s method produced false negatives at regions around the optic disk and pathological lesions. Our proposed methods employ the multidirectional morphological top-hat transformation to enhance the vessels in the retinal image, the optic disk has been removed, and the response to thin vessels is more sensitive. Moreover, in the STARE database, the pathological images are 10 out of 20, and our proposed method has achieved high performance. The average Local Accuracy for the STARE dataset is 0.7642, which approximates the measures of a second human observer. That is because the directional linear structuring elements used in top-hat on the filtered image enhances all vessels, whatever their direction, including small or tortuous vessels, and the large homogeneous pathological areas become normalized.

Our proposed method belongs to an unsupervised segmentation method, which doesn't require ground truth segmentations for training models. Statistics of the running time of the proposed method to segment a DRIVE or STARE image are implemented on a PC Intel Core i5 3.2 GHz CPU and 8 GB RAM. The method is implemented in MATLAB, and no optimization is performed. The image preprocessing phase, including vessel enhancement phase, spends 1.26 seconds on average, and the time to detect vessels by improved multiscale line detection is 2.72 seconds, so it takes 3.98 seconds on average to segment a DRIVE or STARE image, using our proposed method. Being an unsupervised method, it is effective enough, and the execution time could be reduced further by some optimization of our proposed method.

V. CONCLUSIONS

In this paper, an effective retinal blood vessel segmentation method has been proposed. A multidirectional top-hat transform with rotating structuring elements was used to emphasize the vessels. The multidirectional filters have enhanced all vessels, whatever their direction, including small or tortuous vessels. Every isolated round and bright zone whose diameters were less than the length of the linear structuring element pixels have been removed, so the influence of the optic disk and pathological lesions for vessel detection have been decreased. Then, an improved multiscale line detector was proposed to yield vessel responses. Setting different weights to different scale line detectors, our improved multiscale line detector included less background noise into the line responses, which could yield segmentation results with more small vessels. Experimental results have shown that our method can segment these close vessels, and has the ability to deal with these centers of central reflex vessels. Being an unsupervised method, our method has produced comparable accuracy. The demonstrated effectiveness and robustness, together with its simplicity, make the proposed blood vessel segmentation method a suitable tool for being integrated into a computer-assisted diagnostic

Table 2. DFE performance comparison of different line detector methods (DRIVE databases)

Method	Sensitivity	Specificity	Accuracy	Local Accuracy	AUC
Second observer	0.7796	0.9717	0.9473	0.7921	-
Basic line detect	0.7124	0.9563	0.9329	0.7413	0.9496
Nguyen et al.'s method	0.7322	0.9659	0.9407	0.7883	0.9613
Proposed method	0.7354	0.9691	0.9415	0.7896	0.9618

AUC: area under ROC curve, ROC: receiver operating characteristic.

Table 3. Performance comparison of different line detectors methods (STARE databases)

Method	Sensitivity	Specificity	Accuracy	Local Accuracy	AUC
Second observer	0.8951	0.9584	0.9350	0.7706	-
Basic line detect	0.7116	0.9538	0.9356	0.7285	0.9427
Nguyen et al.'s method	0.7317	0.9613	0.9324	0.7630	0.9568
Proposed method	0.7348	0.9652	0.9336	0.7657	0.9576

AUC: area under ROC curve, ROC: receiver operating characteristic.

system for ophthalmic disorders. The majority of the vessels that have not been segmented effectively are those around pathological lesions. To segment those vessels is the subject of ongoing work.

AKNOWLEDGMENTS

This research is supported by the Fundamental Research Foundation of Henan Province, under Grant No.132300410396.

REFERENCES

1. R. Bernardes, P. Serranho, and C. Lobo, "Digital ocular fundus imaging: a review," *Ophthalmologica*, vol. 226, no. 4, pp. 161-181, 2011.
2. M. M. Fraz, P. Remagnino, A. Hoppe, B. Uyyanonvara, A. R. Rudnicka, C. G. Owen, and S. A. Barman, "An ensemble classification-based approach applied to retinal blood vessel segmentation," *IEEE Transactions* on *Biomedical Engineering*, vol. 59, no. 9, pp. 2538-2548, 2012.
3. M. M. Fraz, P. Remagnino, A. Hoppe, and S. A. Barman, "Retinal image analysis aimed at extraction of vascular structure using linear discriminant classifier," in *Proceedings of the International Conference on Computer Medical Applications*, Sousse, Tunisia, 2013, pp. 1-6.
4. U. T. Nguyen, A. Bhuiyan, L. A. Park, and K. Ramamohanarao, "An effective retinal blood vessel segmentation method using multi-scale line detection," *Pattern Recognition*, vol. 46, no. 3, pp. 703-715, 2013.
5. Y. Wang, G. Ji, P. Lin, and E. Trucco, "Retinal vessel segmentation using multiwavelet kernels and multiscale hierarchical decomposition," *Pattern Recognition,* vol. 46, no. 8, pp. 2117-2133, 2013.
6. M. M. Fraz, P. Remagnino, A. Hoppe, B. Uyyanonvara, A. R. Rudnicka, C. G. Owen, and S. A. Barman, "Blood vessel segmentation methodologies in retinal images: a survey," *Computer Methods and Programs in Biomedicine*, vol. 108, no. 1, pp. 407-433, 2012.
7. O. Faust, R. Acharya, E. Y. K. Ng, K. H. Ng, and J. S. Suri, "Algorithms for the automated detection of diabetic retinopathy using digital fundus images: a review," *Journal of Medical Systems,* vol. 36, no. 1, pp. 145-157, 2012.
8. M. M. Fraz, A. Basit, and S. A. Barman, "Application of morphological bit planes in retinal blood vessel extraction," *Journal of Digital Imaging*, vol. 26, no. 2, pp. 274-286, 2013.
9. Q. Li, J. You, and D. Zhang, "Vessel segmentation and width estimation in retinal images using multiscale production of matched filter responses," *Expert Systems with Applications,* vol. 39, no. 9, pp. 7600-7610, 2012.
10. F. Zana and J. C. Klein. "Segmentation of vessel-like patterns using mathematical morphology and curvature evaluation," *IEEE Transactions on Image Processing*, vol. 10, no. 7, pp. 1010-1019, 2001.
11. Y. Yin, M. Adel, and S. Bourennane, "Retinal vessel segmentation using a probabilistic tracking method," *Pattern Recognition*, vol. 45, no. 4, pp. 1235-1244, 2012.
12. F. Nie and P. Zhang, "Fuzzy partition and correlation for image segmentation with differential evolution," *IAENG International Journal of Computer Science*, vol. 40, no. 3, pp. 164-172, 2013.
13. A. Hunter, J. Lowell, R. Ryder, A. Basu, and D. Steel, "Tramline filtering for retinal vessel segmentation," in *Proceedings of the 3rd European Medical and Biological Engineering Conference*, Prague, Czech Republic, 2005, pp. 1-4.
14. E. Ricci and R. Perfetti, "Retinal blood vessel segmentation using line operators and support vector classification," *IEEE Transactions on Medical Imaging*, vol. 26, no. 10, pp. 1357-1365, 2007.
15. M. Niemeijer, J. Staal, B. van Ginneken, M. Loog, and M. D. Abramoff, "Comparative study of retinal vessel segmentation methods on a new publicly available database," in *Proceedings of SPIE*: *Medical Imaging 2004*, Bellingham, WA: SPIE, pp. 648-656, 2004.
16. A. D. Hoover, V. Kouznetsova, and M. Goldbaum, "Locating blood vessels in retinal images by piecewise threshold probing of a matched filter response," *IEEE Transactions on Medical Imaging*, vol. 19, no. 3, pp. 203-210, 2000.
17. J. V. Soares, J. J. Leandro, R. M. Cesar, H. F. Jelinek, and M. J. Cree, "Retinal vessel segmentation using the 2-D Gabor wavelet and supervised classification," *IEEE Transactions on Medical Imaging*, vol. 25, no. 9, pp. 1214-1222, 2006.
18. D. Marin, A. Aquino, M. E. Gegundez-Arias, and J. M. Bravo, "A new supervised method for blood vessel segmentation in retinal images by using gray-level and moment invariants-based features," *IEEE Transactions on Medical Imaging,* vol. 30, no. 1, pp. 146-158, 2011.
19. J. Serra, *Image Analysis and Mathematical Morphology*, London: Academic Press, 1983.

Yanli Hou

Yanli Hou received her B.S. degree in computer applications and M.S. degree in applied mathematics from Henan University in 2002 and 2005, respectively. Her current research interests include image processing technology, pattern recognition, and multi-sensor data fusion technology.